*Geophysical Research Letters*

Supporting Information for

# Regional benthic $\delta^{18}O$ stacks for the "41-kyr world" - an Atlantic-Pacific divergence between 1.8-1.9 Ma

Yuxin Zhou[1], Lorraine E. Lisiecki[1], Taehee Lee[2], Geoffrey Gebbie[3], and Charles Lawrence[2]
[1]Department of Earth Science, University of California, Santa Barbara.
[2]Division of Applied Mathematics, Brown University.
[3]Physical Oceanography Department, Woods Hole Oceanographic Institution.

## Contents of this file



## Text S1 – Basin-wide average normalized sedimentation rate

Over the Pleistocene, we can expect the global average normalized sedimentation rate to be fairly constant (Lisiecki & Raymo, 2005). We monitor the normalized sedimentation rate of our regional stacks when choosing additional age controls (i.e., tie points). To calculate the normalized sedimentation rate, each core's sedimentation rate based on BIGMACS alignment is divided by its mean sedimentation rate, interpolated to 1-kyr intervals, and averaged across all Atlantic or Pacific cores.

## Text S2 – BIGMACS stack construction

In addition to the 1.5-2.1 Ma regional stacks discussed in the main text, we also constructed regional Pleistocene (0-2.7 Ma) stacks for the Atlantic and the Pacific. The construction of these stacks did not involve additional age controls except those identified from the Neptune database (see main text). Because of the intense computational resources required quickly exceed that of even a supercomputer (over 1 TB of RAM), both the Atlantic and the Pacific stacks were constructed in two segments (0-700 ka and 700-2700 ka for the Atlantic; 0-300 ka and 300-2700 ka for the Pacific). The time length of the segments during the more recent past is shorter because more $\delta^{18}O$ records are available, requiring a shorter interval of alignment to keep the use of computational resources reasonable. The overlaps between segments are averaged in stitching together the segments to create a stack for the entire Pleistocene.

BIGMACS stack construction requires an initial alignment target for the initial alignment all of the records, and we used the LR04 global stack (Lisiecki & Raymo, 2005). The software then iteratively updates the stack to which the records are aligned until convergence. We used the default settings for all the hyperparameters (Lee et al., 2023). The stack construction process also

includes core-specific shift and scale parameters that are learned during the alignment using the Baum-Welch Expectation Maximization algorithm.

In constructing the new BIGMACS stacks, we incorporate age estimates from the Neptune Sandbox Berlin (NSB) database (Renaudie et al., 2020), which compiled biostratigraphic and paleomagnetic events from the International Ocean Discovery Program (IODP) and its predecessors. The conversion of NSB hole-specific meters below sea floor (mbsf) depths to meters composite depth (mcd) was done using the IODP Janus Depth Point Calculator. Because the age information provided by the NSB database does not come with uncertainty estimates, we conservatively specify the age uncertainty as Gaussian distributions with a standard deviation of 100 kyr. Due to the large uncertainty for these age constraints, the Atlantic and Pacific stacks mostly follow the age model of the LR04 stack used for the initial alignment target.

**Text S3 – Alternative causes of regional divergence**

Could the regional divergence be solely caused by the light $\delta^{18}O$ input into the Atlantic from the meltwater event alone? We do not find this explanation likely. First, the more recent meltwater events of the last glacial period led to only modest and relatively short-lived differences (4 kyr or less) between regional benthic $\delta^{18}O$ stacks (Lisiecki & Stern, 2016). In contrast, the glacial maximum in the Atlantic stack at 1.878 Ma, is barely identifiable and would probably require a meltwater event of much larger magnitude and duration. Second, Shakun et al. (2016) identified other meltwater events that do not produce the same regional divergences. The meltwater events other than the one at ~1.85 Ma (and possibly another at ~2.05 Ma) are not associated with clear differences in the Atlantic and Pacific benthic $\delta^{18}O$ records and have magnitudes both greater and smaller than the one at 1.85 Ma. Nevertheless, the meltwater event at 1.85 Ma and the associated light $\delta^{18}O$ input could have been a secondary contributing factor that led to the regional benthic $\delta^{18}O$ differences.

An alternative explanation for the Atlantic-Pacific divergence is that the meltwater event led to a foraminifera-barren zone in the Atlantic – a hiatus in the Atlantic benthic $\delta^{18}O$ records that left one or more marine isotope stages unrecorded. For example, foraminifera-barren zones in sediments are observed during Heinrich events of the last glacial cycle (Ruddiman & McIntyre 1981; Broecker et al. 1992; McManus et al. 1998) and the penultimate glaciation (Ruddiman et al. 1980). During these Heinrich events, icebergs and the accompanying meltwater were rapidly discharged into the North Atlantic from the Hudson Strait region during periods of Laurentide Ice Sheet instability (Heinrich 1998; Broecker et al. 1992; Zhou et al., 2021).

However, we find this explanation to be unlikely. While foraminifera dissolution may be an appealing explanation for the Atlantic-Pacific divergence we observed, we do not find a gap in benthic $\delta^{18}O$ measurements at this time or an apparent decrease in Atlantic sedimentation rates during this period (see Fig. S7 for an example using U1308). If a sedimentation hiatus in the Atlantic was responsible for failing to record the majority of a glacial period, we would expect a more discernable drop in the apparent Atlantic sedimentation rates between 1.8-1.9 Ma. If foraminifera dissolution played a role in causing the Atlantic-Pacific benthic $\delta^{18}O$ differences, that role is likely a minor one.

**Text S4 – Visual confirmation of BIGMACS record alignment**

To verify the Atlantic-Pacific difference identified by BIGMACS in record alignment, we developed a strategy to visually confirm the BIGMACS results for certain high-resolution cores during 1.8-1.9 Ma. While most of the glacial cycles in the 41-kyr world repeat the typical sawtooth pattern (gradual buildup and fast termination of ice sheets), some glacial cycles stand out with "double interglacial" or "step interglacial" features. Double interglacials are two interglacial periods interrupted by a weak and short glacial, structurally similar to Marine Isotope Stage 7 in the 100-kyr world (Choudhury et al., 2020). Step interglacials are similar to double interglacials in that two interglacials are interrupted by a weak and short glacial. However, unlike the double interglacials, the step interglacials start with a moderate interglacial followed by a second, comparatively more intense interglacial. The step interglacials represent a two-step transition that is similar to Marine Isotope Stage 13 in the 100-kyr world. The double interglacials and step interglacials before or after 1.8-1.9 Ma can serve as anchor points to contradict or corroborate the algorithmic alignment by BIGMACS during 1.8-1.9 Ma (Fig. S6).

The double interglacials during MIS 61 (~1.725 Ma) and the step interglacials during MIS 77 (~2.025 Ma) serve as useful anchors that can help visually confirm the BIGMACS alignment during 1.8-1.9 Ma (Fig. S6). Between MIS 61 and 1.8 Ma, benthic $\delta^{18}O$ records with sufficient resolution show one climatic cycle. Between MIS 77 and 1.9 Ma, benthic $\delta^{18}O$ records show two climatic cycles. As a result, we have added confidence in the BIGMACS record alignment during 1.8-1.9 Ma. Any discrepancy among records during this period is hard to dismiss as erroneous algorithmic alignment.

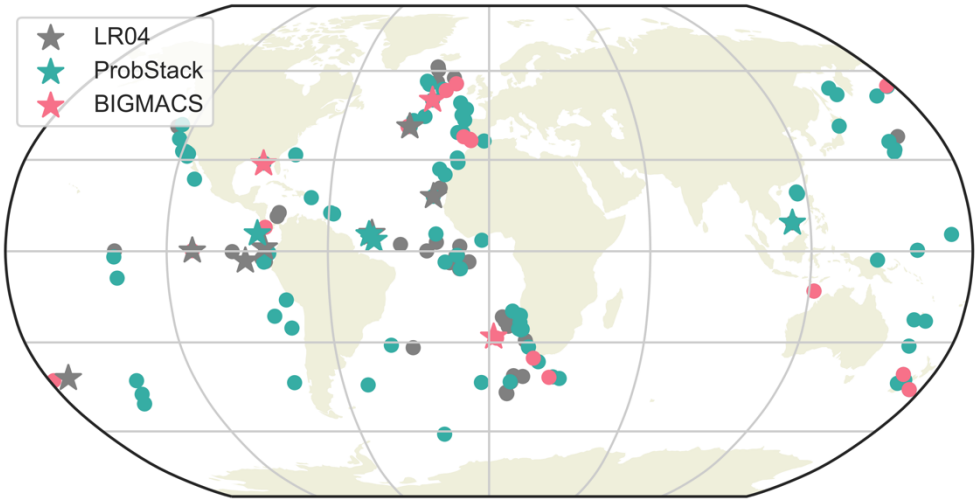


**Figure S1.** Map of the input cores for the BIGMACS Atlantic and Pacific stacks construction, including existing compilations and additional records newly compiled for this study. Stars mark the high-resolution cores shown in Fig. S3 and S4.

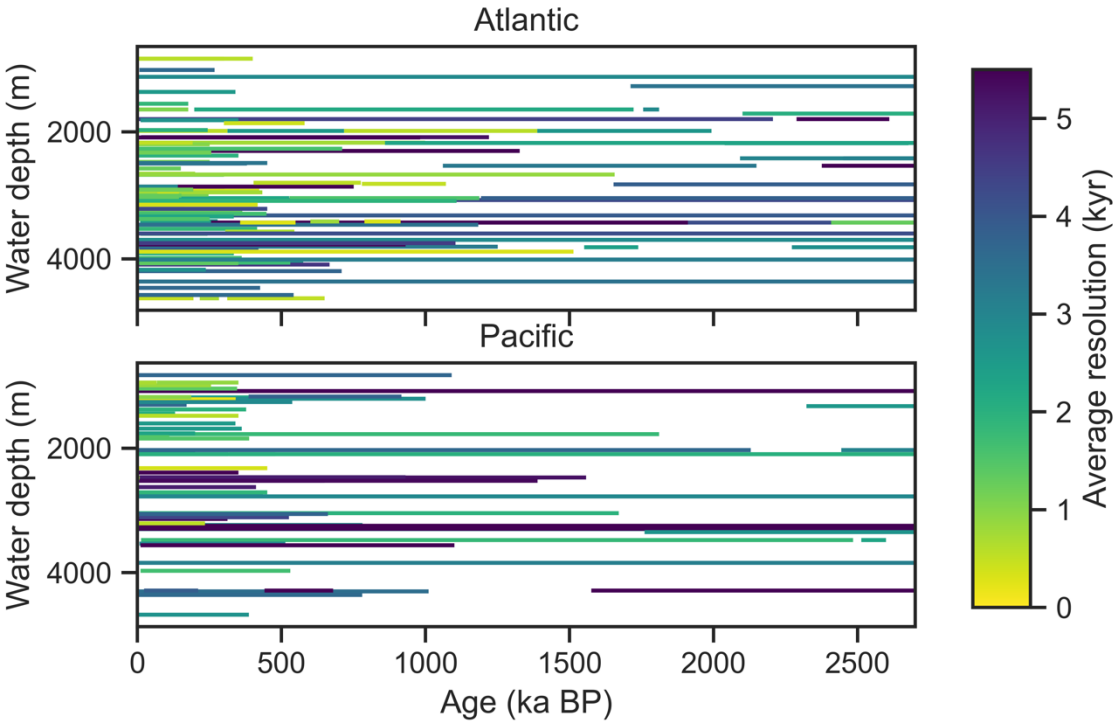


**Figure S2.** Overview of the BIGMACS stack input record water depth, temporal range, and average resolution, divided by ocean basins. Lighter color means the record is more densely measured (i.e., the average time spacing between samples is smaller).

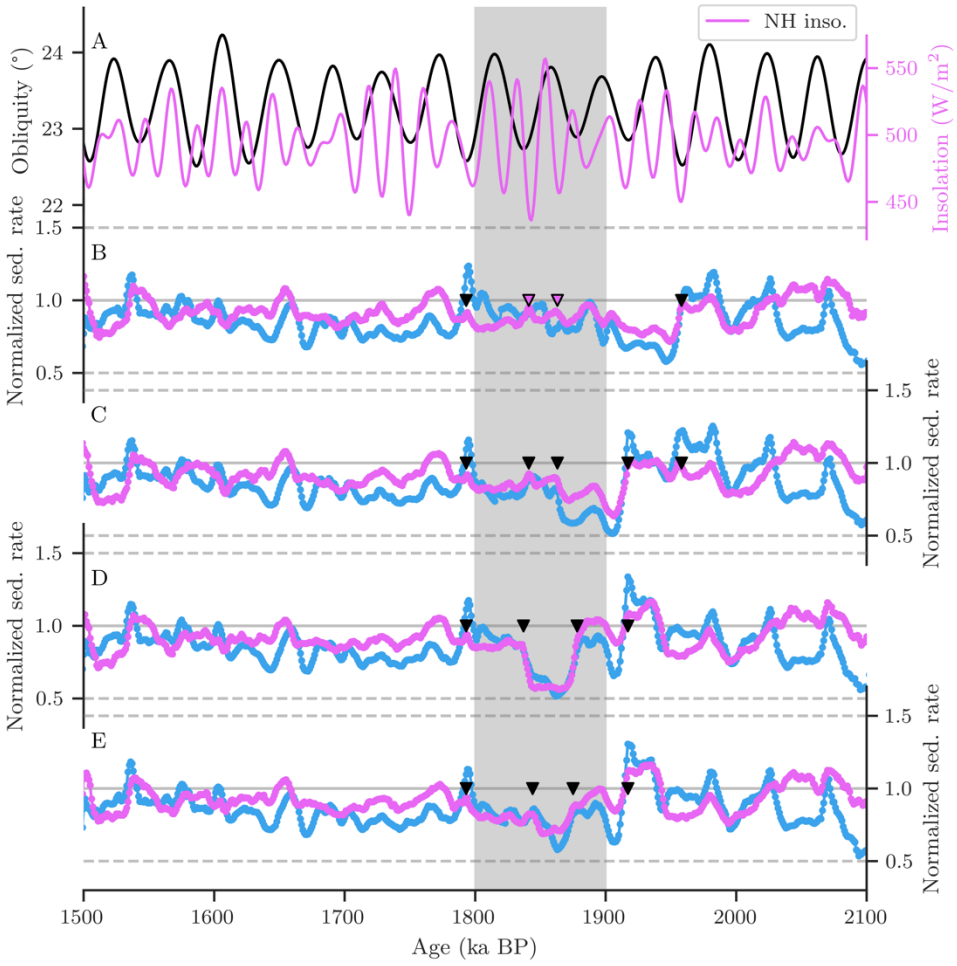


**Figure S3.** Basin-wide normalized sedimentation rates depending on the choices of additional age controls. (**A**) Obliquity (black line) and NH insolation (purple line) at 65° N. (**B-E**) Basin-wide normalized sedimentation rates using different additional age controls imposed on the stack construction (triangles). Purple lines are for alternate versions of the Atlantic regional stacks and blue lines are for Pacific regional stacks. Black triangles mark additional age controls imposed on both stack, and purple triangles mark additional age controls imposed only on the Atlantic stack. The main text shows the stacks constructed using the additional age controls in (B), which produce the smallest variation in normalized sedimentation rates between 1.8-1.9 Ma.

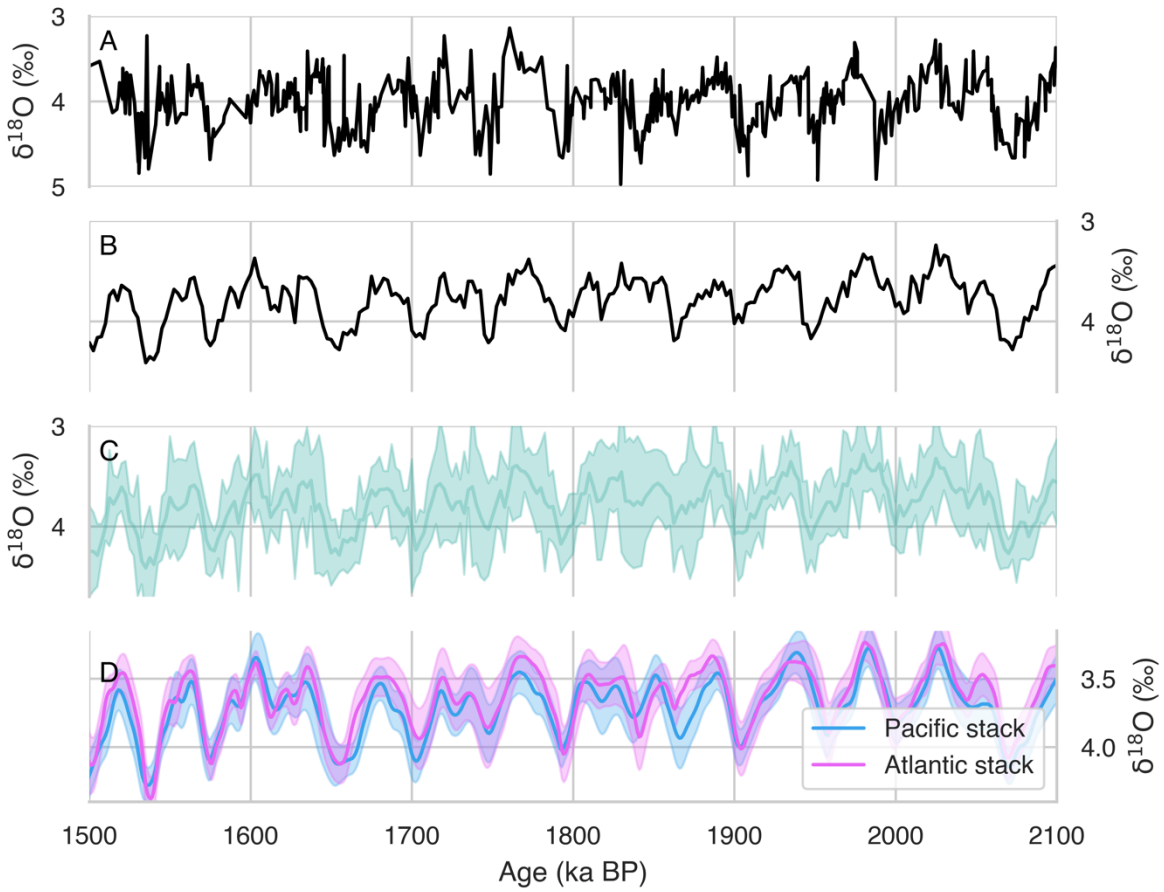


**Figure S4.** Stack comparison between (A) CENOGRID (Westerhold et al., 2020), (B) LR04 (Lisiecki & Raymo, 2005), (C) ProbStack (Ahn et al., 2017), and (D) the 1.5-2.1 Ma regional stacks with tie-point-guided alignments from this study.

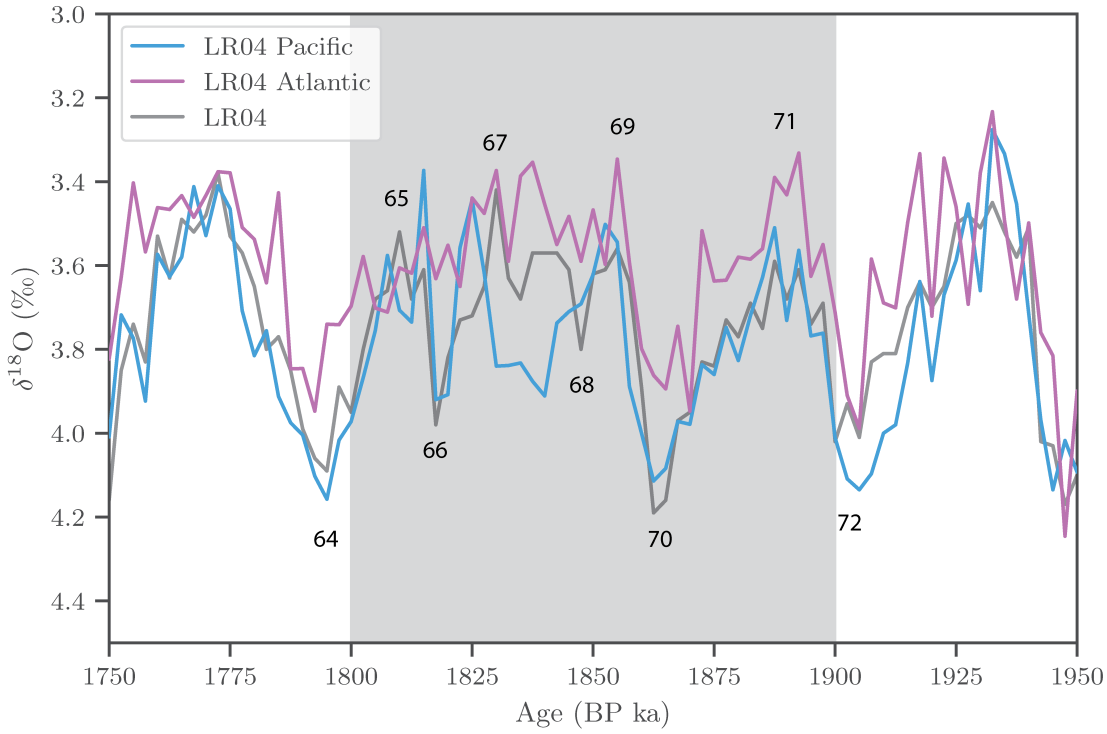


**Figure S5.** The LR04 global stack and separate binned stacks of its component Atlantic and Pacific records (as aligned during LR04 stack construction). The gray shade outlines the 1.8-1.9 Ma period where the Atlantic and the Pacific binned stacks diverge. Numbers denote the Marine Isotope Stages 64-72 in LR04.

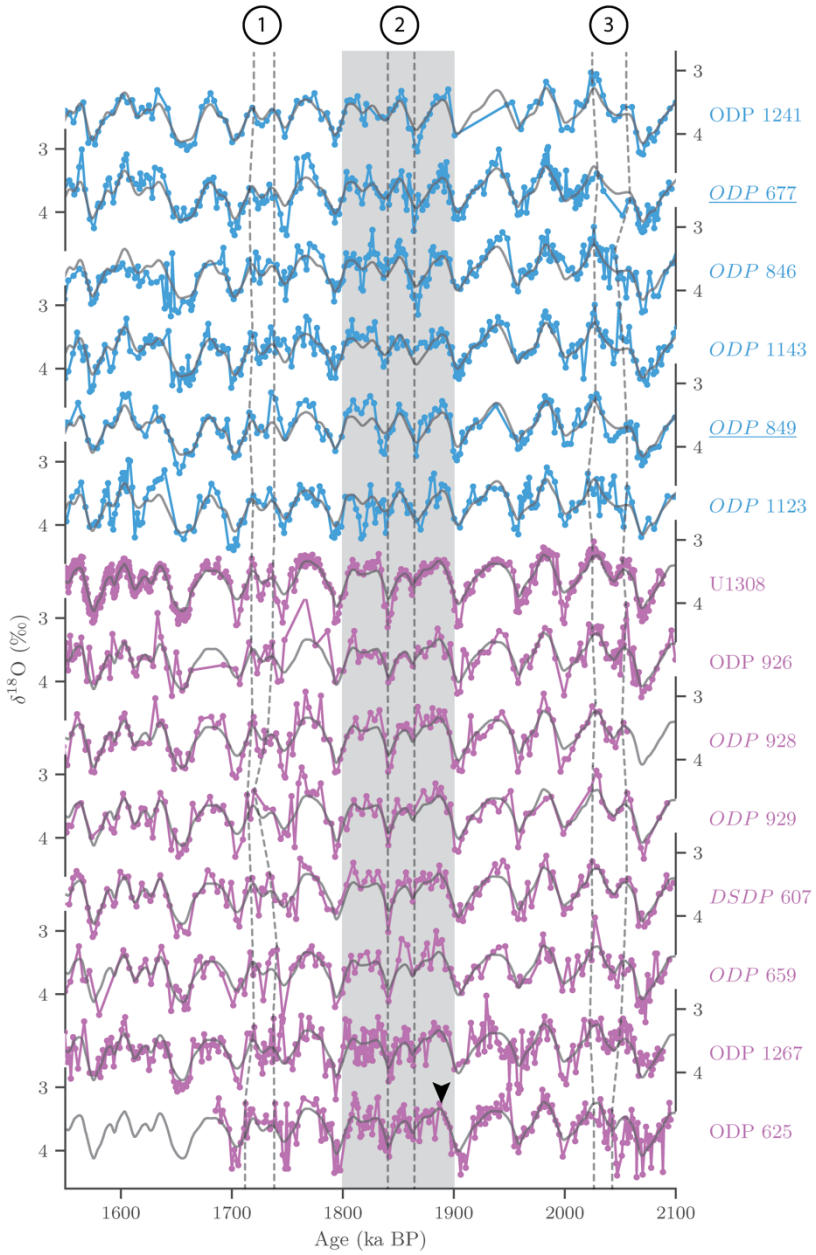


**Figure S6.** Visual confirmation of the BIGMACS alignment of high-resolution benthic $\delta^{18}O$ records. Records are plotted using the medians of age estimates. Blue markers are Pacific records. Purple markers are Atlantic records. Solid gray lines display the BIGMACS regional stacks (Pacific stack for the Pacific records and Atlantic stack for the Atlantic records). Feature 1 and the dashed lines below it mark the double interglacial feature. Feature 3 and the dashed lines below it mark the step interglacial feature. Feature 2 mark the pattern in the Atlantic cores, where a moderate glacial was followed by a second, relatively intense glacial. The gray shade outlines the 1.8-1.9 Ma period where the Atlantic and the Pacific records diverge. The black arrow denotes a meltwater event discovered in ODP 625 (Shakun et al., 2016). The cores with names underlined are the targets used by LR04 for alignment. The cores with names in italic are the records that were used as input for LR04.

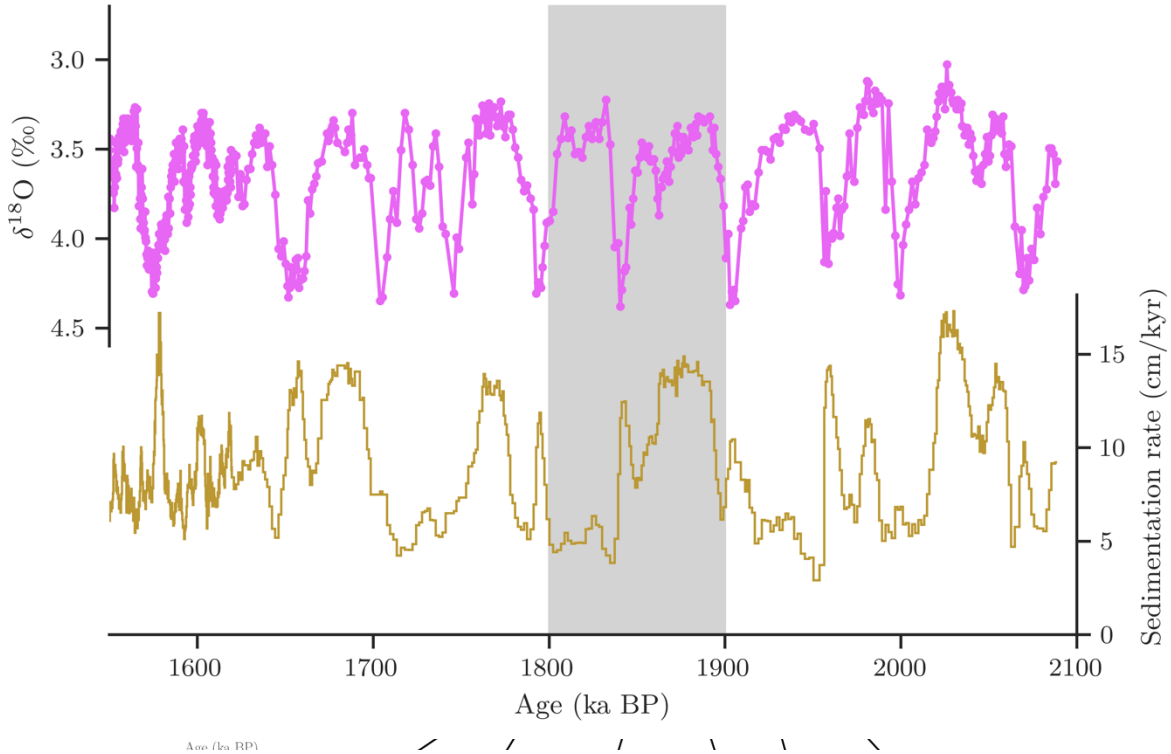


**Figure S7.** U1308 benthic $\delta^{18}O$ and sedimentation rate. Top: U1308 benthic $\delta^{18}O$. Bottom: U1308 sedimentation rate calculated using the BIGMACS alignment age. The gray shade outlines the 1.8-1.9 Ma period where the Atlantic and the Pacific records diverge.

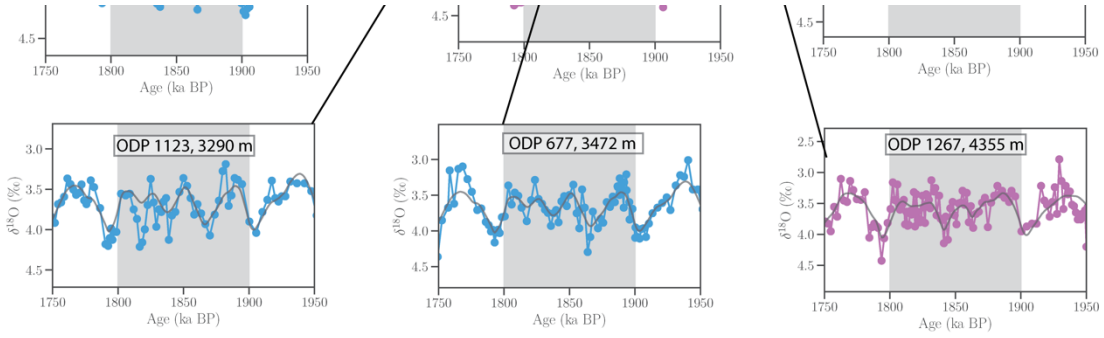


**Figure S8.** Same records as in Fig. S3 but shown with the locations of the cores.

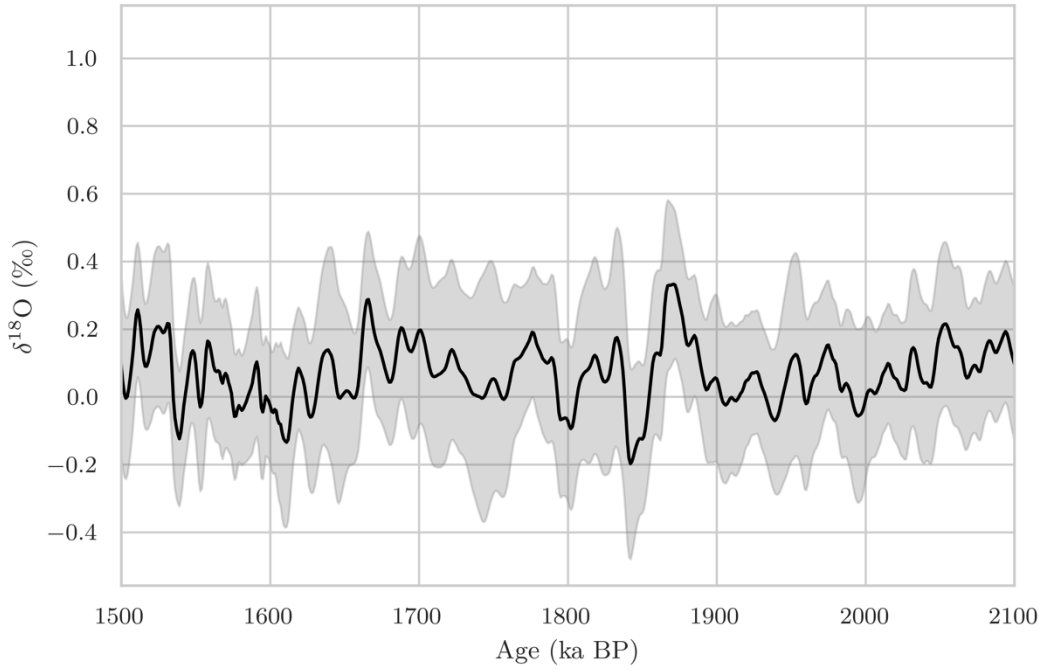


**Figure S9.** Time series difference between the Pacific and Atlantic stacks as shown in Fig. 2B (Pacific-Atlantic).

| | | | | | |
|---|---|---|---|---|---|
| U1313 | 41 | -32.9573 | 3426 | Naafs et al. (2020) | https://doi.org/10.1029/2020PA003905 |
| DSDP610 | 53.2215 | -18.8868 | 2417 | Naafs et al. (2020) | https://doi.org/10.1029/2020PA003905 |
| AP_comp | -41.43 | 24.26 | 2669 | Starr et al. (2021) | https://doi.org/10.1038/s41586-020-03094-7 |
| U1308 | 49.88 | -24.24 | 3883 | Hodell and Channell (2016) | https://doi.org/10.5194/cp-12-1805-2016 |
| U1476 | -15.8 | 41.8 | 2166 | Barker et al. (2022) | https://doi.org/10.1126/science.abm4033 |
| ODP1264 | -28.5327 | 2.8455 | 2507 | Bell et al. (2014) | https://doi.org/10.1002/2014GC005297 |
| ODP1267 | -28.098 | 1.711 | 4355.1 | Bell et al. (2014) | https://doi.org/10.1002/2014GC005297 |

| | | | | | |
|---|---|---|---|---|---|
| DSDP593 | -40.508666667 | 167.674667 | 1080 | McClymont et al. (2016) | https://doi.org/10.1002/2016PA002954 |
| U1483 | -13.0873 | 121.8042 | 1733 | Zhang et al. (2020) | https://doi.org/10.1029/2019JD032125 |
| U1483 | -13.0873 | 121.8042 | 1733 | Gong et al. (2023) | https://doi.org/10.1038/s41467-023-37639-x |
| ODP1125 | -42.55 | -178.17 | 1365 | Caballero-Gill et al. (2019) | https://doi.org/10.1029/2018PA003496 |
| DSDP594 | -45.52 | 174.95 | 1204 | Caballero-Gill et al. (2019) | https://doi.org/10.1029/2018PA003496 |
| ODP1242 | 7.86 | -83.61 | 1363.4 | Diz et al. (2019) | https://doi.org/10.1594/PANGAEA.909154 |
| U1313 | 41 | -32.9573 | 3426 | Catunda et al. (2021) | https://doi.org/10.1594/PANGAEA.932281 |
| U1342 | 54.83 | 176.92 | 818 | Knudson and Ravelo (2015) | https://doi.org/10.1002/2015PA002840 |
| MD01-2444 and U1385 combined | 37.6 | -10.1 | 2621.5 | Hodell et al. (2023) | https://doi.org/10.1594/PANGAEA.951396 |
| U1389 | 36.4 | -7.3 | 644 | Kaboth et al. (2017) | https://doi.org/10.5194/cp-13-1023-2017 |
| U1387 | 36.8 | -7.7 | 558 | Voelker et al. (2022) | https://doi.org/10.3390/atmos13091378 |
| U1467 | 4.85 | 73.3 | 487 | Stainbank et al. (2020) | https://doi.org/10.1016/j.epsl.2020.116390 |
| U1479 | -35.1 | 17.4 | 2626.9 | Zhao et al. (2020) | https://doi.org/10.1016/j.quascirev.2020.106643 |
| U1446 | 19.084 | 85.735 | 1430 | Clemens et al. (2021) | https://doi.org/10.1126/sciadv.abg3848 |
| ODP849 | 0.1823 | -110.519717 | 3839 | Jakob et al. (2021) | https://doi.org/10.1029/2020PA003965 |
| U1313 | 41 | -32.9573 | 3426 | Jakob et al. (2020) | https://doi.org/10.1073/pnas.2004209117 |
| ODP981 | 55.4771833 | -14.6508333 | 2173 | Draut et al. (2003) | https://doi.org/10.1029/2003PA000889 |
| ODP625 | 28.83 | -87.16 | 889 | Shakun et al. (2016) | https://doi.org/10.1002/2016PA002956 |

**Table S1.** Locations and references of records added to the collection by this study.

**References**

Ahn, S., Khider, D., Lisiecki, L. E., & Lawrence, C. E. (2017). A probabilistic Pliocene–Pleistocene stack of benthic $\delta^{18}O$ using a profile hidden Markov model. *Dynamics and Statistics of the Climate System*, *2*(1). https://doi.org/10.1093/climsys/dzx002

Barker, S., Starr, A., van der Lubbe, J., Doughty, A., Knorr, G., Conn, S., et al. (2022). Persistent influence of precession on northern ice sheet variability since the early Pleistocene. *Science*, *376*(6596), 961–967. https://doi.org/10.1126/science.abm4033

Bell, D. B., Jung, S. J. A., Kroon, D., Lourens, L. J., & Hodell, D. A. (2014). Local and regional trends in Plio-Pleistocene $\delta^{18}O$ records from benthic foraminifera. *Geochemistry, Geophysics, Geosystems*, *15*(8), 3304–3321. https://doi.org/10.1002/2014GC005297

Caballero-Gill, R. P., Herbert, T. D., & Dowsett, H. J. (2019). 100-kyr Paced Climate Change in the Pliocene Warm Period, Southwest Pacific. *Paleoceanography and Paleoclimatology*, *34*(4), 524–545. https://doi.org/10.1029/2018PA003496

Catunda, M. C. A. (2021). Oxygen isotope ratios measured on benthic foraminifera of IODP Site 306-U1313 (MIS 14-36) [Text/tab-separated-values]. PANGAEA. https://doi.org/10.1594/PANGAEA.932281

Choudhury, D., Timmermann, A., Schloesser, F., Heinemann, M., & Pollard, D. (2020). Simulating Marine Isotope Stage 7 with a coupled climate–ice sheet model. *Climate of the Past*, *16*(6), 2183–2201. https://doi.org/10.5194/cp-16-2183-2020

Clemens, S. C., Yamamoto, M., Thirumalai, K., Giosan, L., Richey, J. N., Nilsson-Kerr, K., et al. (2021). Remote and local drivers of Pleistocene South Asian summer monsoon precipitation: A test for future predictions. *Science Advances*, *7*(23), eabg3848. https://doi.org/10.1126/sciadv.abg3848

Diz, P., Peñalver-Clavel, I., Hernández-Almeida, I., & Bernasconi, S. M. (2019). Oxygen isotopes of benthic foraminifera of ODP Site 202-1242 [Text/tab-separated-values]. PANGAEA. https://doi.org/10.1594/PANGAEA.909154

Draut, A. E., Raymo, M. E., McManus, J. F., & Oppo, D. W. (2003). Climate stability during the Pliocene warm period. *Paleoceanography*, *18*(4). https://doi.org/10.1029/2003PA000889

Gong, L., Holbourn, A., Kuhnt, W., Opdyke, B., Zhang, Y., Ravelo, A. C., et al. (2023). Middle Pleistocene re-organization of Australian Monsoon. *Nature Communications*, *14*(1), 2002. https://doi.org/10.1038/s41467-023-37639-x

Hodell, D. A., & Channell, J. E. T. (2016). Mode transitions in Northern Hemisphere glaciation: co-evolution of millennial and orbital variability in Quaternary climate. *Climate of the Past*, *12*(9), 1805–1828. https://doi.org/10.5194/cp-12-1805-2016

Hodell, D. A., Crowhurst, S. J., Lourens, L., Margari, V., Nicolson, J., Rolfe, J. E., et al. (2023). A 1.5-million-year record of orbital and millennial climate variability in the North Atlantic. *Climate of the Past*, *19*(3), 607–636. https://doi.org/10.5194/cp-19-607-2023

Jakob, K. A., Wilson, P. A., Pross, J., Ezard, T. H. G., Fiebig, J., Repschläger, J., & Friedrich, O. (2020). A new sea-level record for the Neogene/Quaternary boundary reveals transition to a more stable East Antarctic Ice Sheet. *Proceedings of the National Academy of Sciences*, *117*(49), 30980–30987. https://doi.org/10.1073/pnas.2004209117

Jakob, K. A., Ho, S. L., Meckler, A. N., Pross, J., Fiebig, J., Keppler, F., & Friedrich, O. (2021). Stable Biological Production in the Eastern Equatorial Pacific Across the Plio-Pleistocene Transition (~3.35–2.0 Ma). *Paleoceanography and Paleoclimatology*, *36*(4), e2020PA003965. https://doi.org/10.1029/2020PA003965

Kaboth, S., Grunert, P., & Lourens, L. (2017). Mediterranean Outflow Water variability during the Early Pleistocene. *Climate of the Past*, *13*(8), 1023–1035. https://doi.org/10.5194/cp-13-1023-2017

Knudson, K. P., & Ravelo, A. C. (2015). North Pacific Intermediate Water circulation enhanced by the closure of the Bering Strait. *Paleoceanography*, *30*(10), 1287–1304. https://doi.org/10.1002/2015PA002840

Lee, T., Rand, D., Lisiecki, L. E., Gebbie, G., & Lawrence, C. (2023). Bayesian age models and stacks: combining age inferences from radiocarbon and benthic $\delta^{18}O$ stratigraphic alignment. *Climate of the Past*, *19*(10), 1993–2012. https://doi.org/10.5194/cp-19-1993-2023

Lisiecki, L. E., & Raymo, M. E. (2005). A Pliocene-Pleistocene stack of 57 globally distributed benthic $\delta^{18}O$ records. *Paleoceanography*, *20*(1), 1–17. https://doi.org/10.1029/2004PA001071

Lisiecki, L. E., & Stern, J. V. (2016). Regional and global benthic δ18O stacks for the last glacial cycle. *Paleoceanography*, *31*(10), 1368–1394. https://doi.org/10.1002/2016PA003002

McClymont, E. L., Elmore, A. C., Kender, S., Leng, M. J., Greaves, M., & Elderfield, H. (2016). Pliocene-Pleistocene evolution of sea surface and intermediate water temperatures from the southwest Pacific. *Paleoceanography*, *31*(6), 895–913. https://doi.org/10.1002/2016PA002954

Naafs, B. D. A., Voelker, A. H. L., Karas, C., Andersen, N., & Sierro, F. J. (2020). Repeated Near-Collapse of the Pliocene Sea Surface Temperature Gradient in the North Atlantic. *Paleoceanography and Paleoclimatology*, *35*(5), e2020PA003905. https://doi.org/10.1029/2020PA003905

Renaudie, J., Lazarus, D. B., & Diver, P. (2020). NSB (Neptune Sandbox Berlin): An expanded and improved database of marine planktonic microfossil data and deep-sea stratigraphy. *Palaeontologia Electronica*, *23*(1), 1–28. https://doi.org/10.26879/1032

Shakun, J. D., Raymo, M. E., & Lea, D. W. (2016). An early Pleistocene Mg/Ca-δ18O record from the Gulf of Mexico: Evaluating ice sheet size and pacing in the 41-kyr world. *Paleoceanography*, *31*(7), 1011–1027. https://doi.org/10.1002/2016PA002956

Stainbank, S., Spezzaferri, S., De Boever, E., Bouvier, A.-S., Chilcott, C., De Leau, E. S., et al. (2020). Assessing the impact of diagenesis on foraminiferal geochemistry from a low latitude, shallow-water drift deposit. *Earth and Planetary Science Letters*, *545*, 116390. https://doi.org/10.1016/j.epsl.2020.116390

Starr, A., Hall, I. R., Barker, S., Rackow, T., Zhang, X., Hemming, S. R., et al. (2021). Antarctic icebergs reorganize ocean circulation during Pleistocene glacials. *Nature*, *589*(7841), 236–241. https://doi.org/10.1038/s41586-020-03094-7

Voelker, A. H. L., Rodrigues, T., Trotta, S., Marino, M., & Kuhnert, H. (2022). A Southern Portuguese Margin Perspective of Marine Isotope Stage 47—An Interglacial in the 41 kyr World. *Atmosphere*, *13*(9), 1378. https://doi.org/10.3390/atmos13091378

Westerhold, T., Marwan, N., Drury, A. J., Liebrand, D., Agnini, C., Anagnostou, E., et al. (2020). An astronomically dated record of Earth's climate and its predictability over the last 66 million years. *Science*, *369*(6509), 1383–1387. https://doi.org/10.1126/science.aba6853

Zhang, P., Xu, J., Holbourn, A., Kuhnt, W., Beil, S., Li, T., et al. (2020). Indo-Pacific Hydroclimate in Response to Changes of the Intertropical Convergence Zone: Discrepancy on Precession and Obliquity Bands Over the Last 410 kyr. *Journal of*

*Geophysical Research: Atmospheres*, *125*(14), e2019JD032125. https://doi.org/10.1029/2019JD032125

Zhao, X., Koutsodendris, A., Caley, T., & Dupont, L. (2020). Hydroclimate change in subtropical South Africa during the mid-Piacenzian Warm Period. *Quaternary Science Reviews*, *249*, 106643. https://doi.org/10.1016/j.quascirev.2020.106643